Applied Catalysis B: Environmental 129 (2013) 556–565

Contents lists available at SciVerse ScienceDirect

Applied Catalysis B: Environmental

journal homepage: www.elsevier.com/locate/apcatb

Influence of synthesis parameters on the performance of CeO_2–CuO and CeO_2–ZrO_2–CuO systems in the catalytic oxidation of CO in excess of hydrogen

Elisa Moretti[a], Maurizio Lenarda[a,*], Piero Riello[a], Loretta Storaro[a], Aldo Talon[a], Romana Frattini[a], Alvaro Reyes-Carmona[b], Antonio Jiménez-López[b], Enrique Rodríguez-Castellón[b]

[a] Dipartimento di Scienze Molecolari e Nanosistemi, Università Ca' Foscari di Venezia, Via Torino 155/B, 30172 Venezia, Italy
[b] Departamento de Química Inorgánica, Cristalografía y Mineralogía (Unidad Asociada al ICP-CSIC), Facultad de Ciencias, Universidad de Málaga, Campus de Teatinos, E-29071 Málaga, Spain

ARTICLE INFO

Article history:
Received 18 June 2012
Received in revised form 10 October 2012
Accepted 14 October 2012
Available online 23 October 2012

Keywords:
Hydrogen
CO-PROX
Copper
Ceria
Ceria–zirconia
Flower-like morphology

ABSTRACT

Ce–Cu and Ce–Zr–Cu oxide systems with a flower-like morphology were prepared by slow co-precipitation in the absence of any structure directing agent. For the sake of comparison, Ce–Cu and Ce–Zr–Cu oxide samples were also prepared by a classic co-precipitation method. All the samples were calcined in air flow at 650 °C. The materials were characterized by SEM and TEM microscopy, quantitative X-ray diffraction, N_2 physisorption, H_2-TPR, O_2-TPD and XPS. The catalytic activity of the prepared samples was evaluated in the preferential oxidation of CO in excess of H_2 (CO-PROX), in the 40–190 °C temperature range.

© 2012 Elsevier B.V. All rights reserved.

1. Introduction

A multi-component heterogeneous catalyst is usually the association of one or more transition metals with one or more oxides, the activity and selectivity of which is determined by numerous factors. Nevertheless the complete control of the design and synthesis of these systems is still quite far from being achieved and the usual synthetic methods give often difficult to characterize catalytic materials. In fact the catalytic properties of a material depend not only on the chemical nature of the components and their ratio but also on the particles dimension and even on their nano-or micro morphology, all strongly influenced by the preparation method. [1,2]

In the previous years the demand has grown for environment benign catalytic systems related to low-temperature renewable energy production. Catalytic CO oxidation with oxygen in the presence of an excess of H_2 (CO-PROX), is one of the most economical and efficient approaches to reduce the CO content of the H_2-rich gas streams produced by reforming of alcohols or hydrocarbons down to ppm level [3].

Some years ago, Liu and Flytzani-Stephanopoulos [4] reported the extraordinary activity of the CuO–CeO_2 system in the elimination of CO at relatively low temperatures. Now, it is known that the high performances of CuO–CeO_2 based catalysts are attributable to the strong interaction between highly dispersed copper species and the ceria surface, which favors the formation of oxygen vacancies at the copper–ceria boundaries, thus increasing the Cu reducibility [5–9]. It is also known that addition of Zr to ceria modifies the redox properties, the oxygen-storage capacity and thermal resistance of the latter [8,10–16].

The performance of these three-component catalysts, in comparison with CuO–CeO_2 and CuO–ZrO_2 binary systems, was found strongly dependent not only from the molar ratio among reagents but also from the preparation methodology, that can influence the morphological and structural characteristics of the materials as well as the interaction between the oxides and the dispersion of the active phase [17–22]. It was also found that the catalytic behavior of nanostructured ceria, can be significantly influenced by the sample morphology [23–27].

Nanostructures with a 3-dimensional flower-like morphology have been described for various oxides: a flower-like $Ce_{1-x}Zr_xO_2$ solid solution was electrochemically grown [28], well formed flower-like nano-architectures of Cu_xO [29,30], ZnO [31–33], Fe_2O_3 [34], Co_3O_4 [35], MnO_2 [36] and La, Pr doped CeO_2 [37] have been prepared by slow hydrothermal processes.

* Corresponding author. Tel.: +39 0412348562; fax: +39 0412346735.
E-mail address: lenarda@unive.it (M. Lenarda).

0926-3373/$ – see front matter © 2012 Elsevier B.V. All rights reserved.
http://dx.doi.org/10.1016/j.apcatb.2012.10.009

In a previous paper [38], we described the preparation and CO-PROX catalytic activity of a nanostructured Ce/Zr/Cu oxide system with a flower-like morphology. Before catalytic testing, the sample was thermally pre-treated at various temperatures in the 350–650 °C range and it was found that the thermal treatment induces only slight structural changes without altering the overall morphology. The sample treated at 650 °C showed the better CO-PROX activity.

In this work we report the preparation of Ce–Cu and Ce–Zr–Cu mixed oxide systems by slow co-precipitation in the absence of any structure directing agent and by a traditional co-precipitation method. The catalytic performance in the CO Preferential Oxidation of the four obtained samples, previously pretreated at 650 °C, was tested.

2. Experimental

2.1. Reagents

All the materials used are Aldrich products and no further purification was carried out.

2.2. Preparation of the CeCu and CeZrCu based oxide systems

2.2.1. Method (1): Slow co-precipitation

A 0.30 M aqueous solution of K_2CO_3 was slowly added (0.4 mL min^{-1}) to an aqueous solution of $CuCl_2{\cdot}2H_2O$ (1.4 mmol) and $CeCl_3{\cdot}7\ H_2O$ (8.1 mmol) (in the case of CeCu) and to an aqueous solution of $CuCl_2{\cdot}2H_2O$ (1.4 mmol), $CeCl_3{\cdot}7H_2O$ (8.1 mmol) and $ZrOCl_2{\cdot}8H_2O$ (0.9 mmol) (in the case of CeZrCu) under stirring, until a pH value of 8.2 was reached. The suspension was allowed to settle for 20 h, then centrifuged. The resulting solid was washed with deionized water till the complete disappearance of chlorides ($AgNO_3$ test). Both samples were dried overnight at 80 °C and calcined up to 650 °C for 5 h (3 °C min^{-1}).

The samples are identified by the acronyms FCCu and FCZCu, where: F = flower-like; C = cerium; Z = zirconium (if present); Cu = copper.

2.2.2. Method (2): Traditional co-precipitation

This preparation procedure is exactly alike that described in Method (1) with the only difference being that the addition of aqueous solution of K_2CO_3 0.30 M was carried out rapidly (10 mL min^{-1}). The two samples were identified by the acronyms CCu and CZCu respectively.

The metal content was determined by ICP-OES elemental analysis. For the samples FCCu and CCu the CeO_2 content was calculated as 92.9 wt.% and the CuO content was calculated as 7.1%; for the samples FCZCu and CZCu the CeO_2 content was calculated as 86.0 wt.%, the ZrO_2 as 7.0 wt.% and the CuO as 7.0 wt.%.

A very small amount of chlorine was detected in the XPS survey spectra of samples containing zirconium (FCZCu and CZCu).

2.3. Catalytic activity measurements

Catalytic activity tests were carried out in a laboratory flow apparatus with a fixed bed reactor operating at atmospheric pressure. The catalyst, with a defined particle size (0.050–0.110 mm), was introduced into a tubular Pyrex glass reactor (5 mm i.d.), placed in an aluminum heating block.

Before the catalytic experiments, the sample was heated in situ at 400 °C under flowing filtered atmospheric air for 1 h. The gas hourly space velocity (GHSV) was 22,000 h^{-1}. The feed consisted of 1.25% CO, 1.25% O_2 and 50% H_2 (vol.%) balanced with He. Calibration of the GC was done with a gas mixture containing 1% CO, 1% CO_2, 1% O_2 in He.

The effect of CO_2 and H_2O was examined adding both CO_2 (15 vol.%) and H_2O (10 vol.% to the reaction stream using a HPLC pump (Jasco). The GC calibration, when the gas feed was CO_2 rich, was done with 15 vol.% CO_2 in He. The gas lines were heated at 120 °C, to avoid water condensation before the reactor inlet. An ice-cooled water condenser was used to trap the excess of water downstream of the reactor. A HP6890 GC gas chromatograph equipped with a thermal conductivity detector was used to analyze the outlet composition. A CP Carboplot P7 column was used, with helium as carrier. The detection limit for CO was 10 ppm. The temperature was varied in the 40–190 °C range, and measurements were carried out till a steady state was achieved. Both methanation and reverse water-gas-shift reactions were found to be negligible in the experimental conditions. The carbon monoxide and oxygen conversions were calculated based on the CO (Eq. (1)) and O_2 (Eq. (2)) consumption, respectively:

$$\text{CO conversion}(\%) = \frac{n_{CO}^{in} - n_{CO}^{out}}{n_{CO}^{in}} \times 100 \quad (1)$$

$$O_2\ \text{conversion}(\%) = \frac{n_{O_2}^{in} - n_{O_2}^{out}}{n_{O_2}^{in}} \times 100 \quad (2)$$

The selectivity toward CO_2 was estimated from the oxygen mass balance as follows (Eq. (3)):

$$\text{Selectivity}(\%) = \frac{n_{CO}^{in} - n_{CO}^{out}}{2(n_{O_2}^{in} - n_{O_2}^{out})} \times 100 \quad (3)$$

The excess oxygen factor (λ) is defined as (Eq. (4)):

$$\lambda = 2\frac{n_{O_2}^{in}}{n_{CO}^{in}} \quad (4)$$

2.4. Characterization techniques

Inductively coupled plasma (ICP-OES) analyses were performed with a PerkinElmer Optima 3100 XL spectrometer.

X-ray powder diffraction patterns (XRPD) were obtained using a Philips X'Pert system with a Cu Kα radiation (λ = 1.54184 Å). The samples were disc shaped pressed powders and spectra were collected after calcination. The average dimension of the crystallites was determined by the Warren–Averbach's equation (the estimated errors are 10% ca.).

Nitrogen adsorption–desorption measurements were performed at liquid nitrogen temperature (−196 °C) with an ASAP 2010 apparatus of Micromeritics. Before each measurement, the samples (0.1 g) were outgassed first at 130 °C for 12 h at 5×10^{-3} Torr and then at room temperature for 2 h at 0.75×10^{-6} Torr. The N_2 isotherms were used to determine the specific surface areas through the BET equation ($S.A._{BET}$), and the specific pore volume (V_s) calculated at P/P_0 = 0.98.

Scanning electron microscopy (SEM) images were taken with a JEOL JSM-5600LV, operated at 20 kV and using secondary electrons to form the image. The samples were coated with a thin layer of gold.

Transmission electron microscopy (TEM) images were taken on a JEOL-JEM 3010 high-resolution microscope (point resolution at Scherzer defocus 0.17 nm), equipped with a lanthanum hexaboride (LaB6) gun, using an accelerating voltage of 300 kV. The images were taken with a CCD camera (Gatan, mod. 694). The powder was suspended in isopropyl alcohol and dropped on a holey carbon film grid.

Hydrogen temperature-programmed reduction (H_2-TPR) experiments were carried out using an AUTOCHEM 2910 instrument from Micromeritics. Approximately 0.1 g of freshly calcined catalyst were placed on top of some wool glass in a quartz reactor.

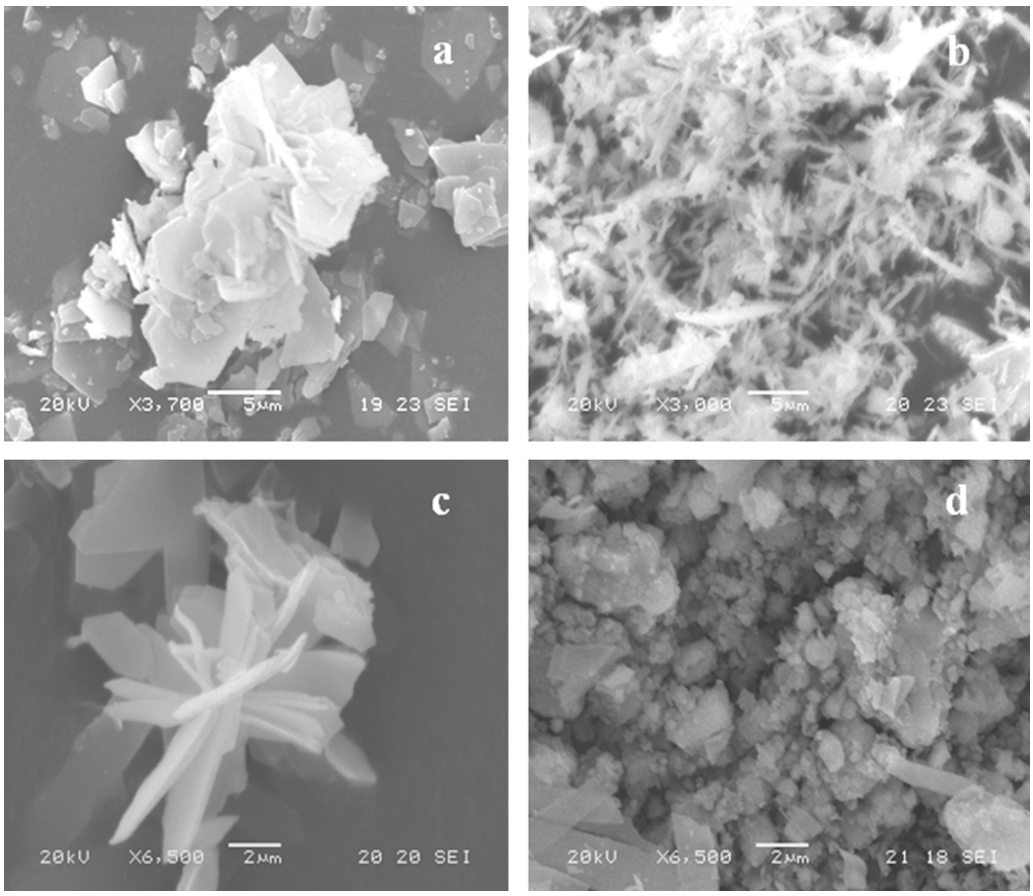

Fig. 1. Scanning electron micrographies of the samples treated at 650 °C: (a) FCCu; (b) CCu; (c) FCZCu and (d) CZCu.

In order to remove contaminants, the powder was pre-treated in helium (20 $cm^3\ min^{-1}$) to 350 °C for 1 h. After cooling to ambient temperature, the TPR experiments were carried out in 10 vol.% H_2/Ar (30 $cm^3\ min^{-1}$) increasing the temperature from 40 °C to 800 °C (10 °C min^{-1}), by a temperature programmable controller. A Dewar flask containing a liquid nitrogen/ethanol slurry was used as cryogenic trap to prevent water to contact the detector.

Oxygen temperature-programmed desorption (O_2-TPD) data were obtained with a Micromeritics TPD/TPR AUTOCHEM 2910 analyzer. Before the measurements, the sample (50 mg) was activated in flowing He at 400 °C for 30 min, cooled to 80 °C and then exposed to 10 vol.% O_2/He flow (20 $cm^3\ min^{-1}$) till 600 °C (20 °C min^{-1}) and left in O_2/He flow at 600 °C for 30 min. The samples were then cooled at 80 °C and purged with He flow for 1 h to remove the physisorbed oxygen before starting the analysis. Finally the TPD experiments were performed flowing He (10 $cm^3\ min^{-1}$) from 80 °C to 900 °C (10 °C min^{-1}).

X-ray photoelectron spectra (XPS) were collected using a Physical Electronics PHI 5700 spectrometer with non monochromatic Mg Kα radiation (300 W, 15 kV, 1253.6 eV) for the analysis of the core level signals of C 1s, O 1s, Zr 3d, Ce 3d and Cu 2p and with a multichannel detector. Spectra of powdered samples were recorded with the constant pass energy values at 29.35 eV, using a 720 μm diameter analysis area. During data processing of the XPS spectra, binding energy values were referenced to the C 1s peak (284.8 eV) from the adventitious contamination layer.

The PHI ACCESS ESCA-V6.0 F software package was used for acquisition and data analysis. A Shirley-type background was subtracted from the signals. Recorded spectra were always fitted using Gauss–Lorentz curves, in order to determine the binding energy of the different element core levels more accurately. The error in BE was estimated to be ca. 0.1 eV. Short acquisition time of 10 min was used to examine C 1s, Cu 2p and Cu LMM XPS regions in order to avoid, as much as possible, photoreduction of Cu^{2+} species. Nevertheless, a Cu^{2+} reduction in high vacuum during the analysis cannot be excluded [39].

3. Results and discussion

3.1. Scanning (SEM) and transmission (TEM) electron microscopies

The surface morphology of the obtained samples was investigated by scanning electron microscopy (SEM) (Fig. 1a–d). A general view of the materials revealed that both samples prepared by slow precipitation, FCCu and FCZCu, present a flower-like morphology, made up by micro-sheets with quite homogeneous size and shape (Fig. 1a and c). The petals are about 200 nm thick and about 10 μm long.

The exact mechanism for the formation of these petals is still unclear, but it is generally suggested that, during a non-template synthesis, the growth of the flower-like morphology is due to homocentric self-assembling from first formed 2D arrangements under control of various factors, such as electrostatic and dipolar fields, van der Waals forces, hydrophobic interactions and hydrogen bonds [29,34,35].

On the other hand both CCu and CZCu sample, prepared by a usual co-precipitation method, did not show any ordered morphology (Fig. 1b and d).

The two materials with a flower-like morphology were further characterized by transmission electron microscopy (TEM).

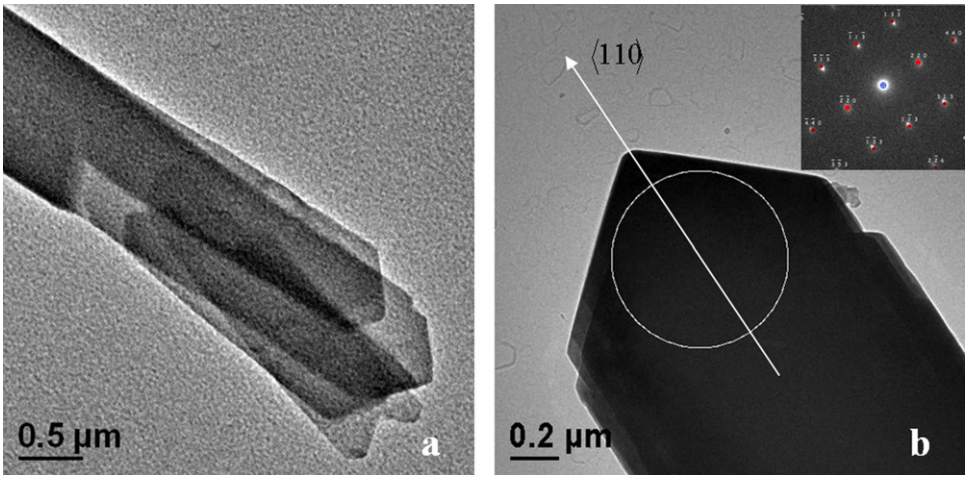

Fig. 2. TEM images of the sample FCZCu: the crystal is ascribed to the more abundant ceria-rich cubic phase (see main text), (a) low-magnification image; (b) magnified image, with SAED (inset): zone axis ⟨3̄32⟩.

A low-magnification TEM image for the sample FCZCu (Fig. 2a) shows a structure made up of individual micro-layers with a preferred growth direction along ⟨110⟩.

The magnified image (Fig. 2b) shows a crystal tip and the electron diffraction data in a selected area are reported in the inset. The exact area where the diffraction spectrum was collected is marked in Fig. 2b, by a white circle. In the inset of Fig. 2b a simulated diffraction pattern with zone axis ⟨3̄32⟩ is superimposed on the experimental one, the former having been calculated with Java Electron Microscopy Software (jems) Version 3.5331U2010 (Copyright: P. Stadelmann, 1999–2010).

The comparison between the orientations of the crystal and its diffraction spectrum confirmed the crystal growth along the ⟨110⟩ crystallographic direction.

3.2. X-ray powder diffraction

Wide-angle XRD was used to identify crystallographic phases of the samples prepared using different experimental conditions.

The diffraction patterns of the two Ce–Cu based materials (Fig. 3a) show the characteristic reflections of fcc CeO_2 with the fluorite structure, as expected for this type of oxide (No. 43-1002 in JCPDS database).

The size of the cubic cerium oxide crystallites in the samples CCu and FCCu have been calculated by the Warren–Averbach analysis of the diffraction lines and found to be very similar, 11.5 and 12.5 nm respectively.

The main peaks of ceria, in the diffractograms of Ce–Zr–Cu based materials, show shoulders (see inset of Fig. 3a), that can be assigned to ZrCe solid solutions $Zr_xCe_{(1-x)}O_2$. It is possible to obtain by Rietveld analysis, using the Vegard law, quantitative information on the composition and distribution of CeO_2 and ZrO_2 in solid solutions. The details of this analysis have been reported in our previous paper [38]. Two different phases were identified in the FCZCu sample XRD profile: a cubic $Zr_xCe_{(1-x)}O_2$ with a low zirconia content and a zirconia-enriched tetragonal one (Fig. 3a). The same quantitative phase composition is found also in the morphologically disordered sample CZCu (Fig. 3a).

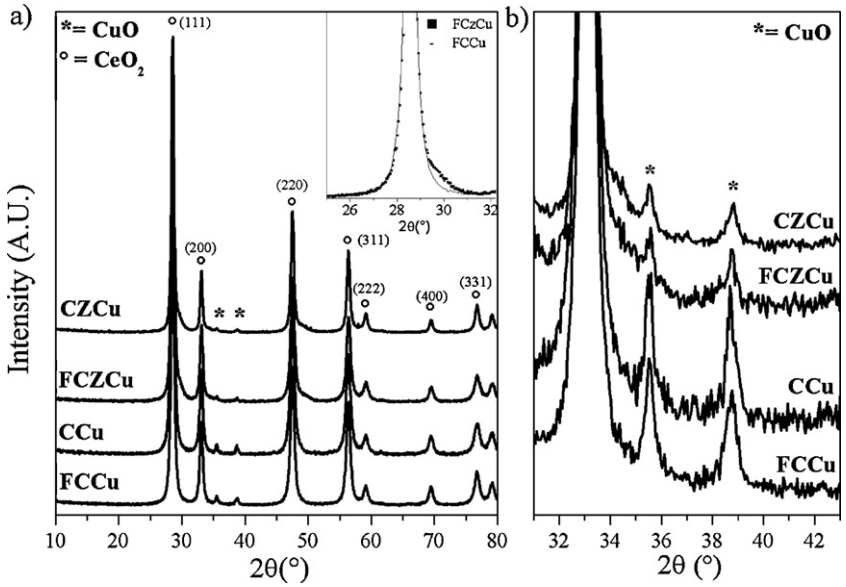

Fig. 3. (a) XRPD patterns of the FCCu, FCZCu, CCu and CZCu samples. In the inset, the comparison of the main peak of ceria for the catalysts FCZCu and FCCu is shown. (b) Enlargement of the XRD profile of the indicated samples in the Cu region.

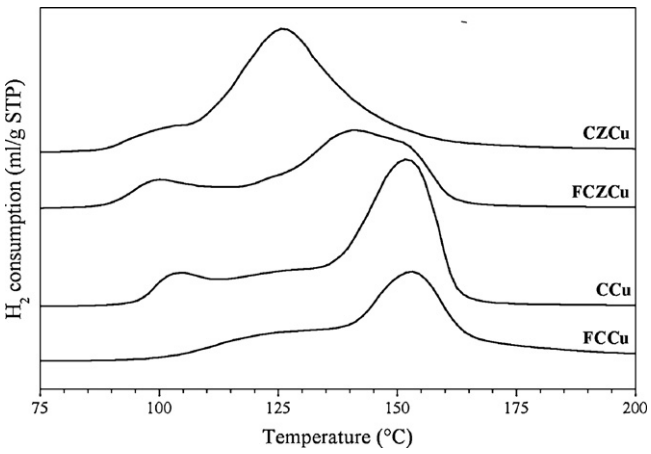

Fig. 4. H_2-TPR profiles of the indicated samples.

The more abundant (86 wt.%) ceria-rich cubic phase, has a composition very close to pure cubic cerianite ($x = 0.02$ ca.) while in the less abundant (about 10 wt.%) zirconia-rich phase the x value is 0.6 ca.). The cubic phase has crystallites of 20.0 nm and the tetragonal of 14.0 nm.

All the XRD profiles (Fig. 3) exhibit small peaks at $2\theta = 35.5°$ and 38.5°, attributed to CuO as tenorite (No. 01-089-2529 in JCPDS database). The diffraction patterns (Fig. 3b) of the two Ce–Cu based materials CCu and FCCu, show that in CCu, the crystallites of CuO with a size of 18.0 nm, represent the 70% of the total copper (Cu as CuO is the 7.1% (w/w) of the total sample weight) while in FCCu the 97% of all the copper is present as CuO crystallites with an average size of 14.0 nm. On the other hand the Ce–Zr–Cu based systems appear to have a smaller fraction of copper present as CuO nanocrystals: 31% in CZCu and 34% in FCZCu, with diameters of 18.0 and 20.0 nm respectively. Since the calculated amount of CuO is, for all the samples, 7% (w/w) it follows that a more or less large fraction of copper oxide large fraction of copper oxide could be present as XRD undetectable very small nanoparticles, substitutional copper ions in the ceria lattice or, owing to the small size of the Cu^{2+} ion, as interstitial punctual defects [40].

This finding further confirms, in agreement with the literature [11,12,17,19,21,41,42], that addition to ceria of even very small amounts of zirconia causes a considerable increase of the metal phase dispersion.

3.3. Hydrogen temperature programmed reduction (H_2-TPR) and oxygen temperature programmmed desorption (O_2-TPD)

The H_2-temperature programmed reduction and the H_2-TPR profiles of the fresh calcined samples are displayed in Fig. 4 while the corresponding H_2 consumption values are reported in Table 1.

Owing to the widely recognized difficulty to resolve, in this kind of experiments, the possible sequential copper reduction ($Cu^{2+} \rightarrow Cu^{+} \rightarrow Cu^{0}$), the different features observed in the TPR profiles must be attributed to the reduction of oxidized copper species with different structural/morphological properties [43]. The H_2-TPR profiles of all the studied samples (Fig. 4) are formed by partially overlapped reduction peaks in the range 100–165 °C, indicating that at least two types of copper species are present. On the other hand CeO_2 shows a very broad peak centered at about 750 °C (not shown in figure), that most probably accounts for reduction of cerium ions of medium–large ceria crystallites [44–46]. The experimental H_2/Cu molar ratio (Table 1) points out that the experimental H_2 consumption is higher than the value expected for the total reduction of Cu^{2+} to Cu^{0}. This additional hydrogen consumption in the H_2-TPR of copper doped ceria was found by various authors and reported in very careful quantitative studies [44,45,47]. This finding was related by Zimmer et al. [47] to hydrogen adsorption on ceria surface, by Pintar et al. [45] to some hydrogen storage in the catalyst structure, while Caputo et al. [44] confirmed that H_2 is adsorbed on CuCe catalysts only after a reducing pre-treatment. Pérez-Hernández et al. [48] suggested that the observed much higher than expected hydrogen uptake during TPR analysis of Ce–Cu systems could be associated to spill over of hydrogen on the support surface that induces concurrent reduction of both copper oxide and ceria. In general it appears to be widely accepted in the literature that the addition of even small amounts of copper species to ceria strongly modifies the redox properties of both constituents of the catalytic system, compared to the pure materials.

The H_2-TPR profile of some of the Cu/Ce and Cu/Zr/Ce oxide systems described in the literature [17,21,43,45,49,50] is usually composed by two well-separated reduction peaks assignable to the reduction of at least two different kind of copper components.

Because H_2-TPR measurements are strongly dependent on the experimental conditions, in this work, we will focus only on the temperature range and on the quantitative comparative evaluation of hydrogen consumption between the samples, in an homogeneous series of experiments. Zimmer et al. [47] quantitatively analyzing hydrogen adsorption and water evolution in the stepwise copper reduction in a CuO/CeO_2 system, found three peaks at 97, 147, and 157 °C respectively. These authors proposed that the complete reduction of copper with hydrogen in a Cu/Ce system involves low temperature (ca. 100 °C) hydrogen adsorption on the ceria active surface catalyzed by CuO and reduction of oxidized copper, ending below 180 °C.

In a previous paper [38] we discussed the effect of thermal pretreatments in the 350–650 °C temperature range on the catalytic behavior in the CO PROX, of the sample FCZCu. Since the sample treated at the highest temperature was found to give the most interesting catalytic performance, the four samples described in this work were all pretreated at 650 °C.

All samples showed quite complex H_2-TPR profiles (Fig. 4), reflecting the heterogeneity of the present copper species.

The Cu reduction process, for all the samples, starts at about 100 °C and can be considered completed below 170 °C, indicating that copper is prevailingly present as highly reducible species. The hydrogen consumption in the 95–125 °C range is attributable to hydrogen adsorption on active surface sites and to the reduction of Cu ions highly dispersed in the ceria lattice [38,51].

Weak hydrogen consumption peaks in the 95–125 °C temperature range are evident in the TPR profiles of CZCu, FCZCu, and CCu, while no peaks of this kind are observable in the profile of FCCu for which the reduction process appears to start only at higher temperature. It can also be observed that, for the Zr containing samples CZCu and FCZCu, the reduction process not only can be considered complete below 160 °C, but the hydrogen consumption peaks are observed in the 125–150 °C range. In particular the curve of CZCu is characterized by a strong peak at about 125 °C attributable to the reduction of ceria associated small clusters that appear to be the most abundant Cu species present in this sample. The FCZCu profile is more complex, the larger hydrogen consumption peak being centered at 140 °C with a tail at higher temperature. These data further confirm that addition of zirconium to ceria enhances both the copper and the oxygen mobility, causing a remarkable increase of the metal phase dispersion.

The strong peak centered at 150 °C indicates that a large part of copper of the non containing Zr samples CCu (70%) and FCCu (97%) is present as XRD detectable well formed (Fig. 3, Table 3) CuO crystals, while only the 30% and 3%, respectively, of total copper is present as very small XRD undetectable copper species (see also Section 3.2).

Table 1
N_2 physisorption data (specific surface area and pore volume), TPR data (H_2 consumption and H_2/Cu molar ratio) and TPD data (O_2 desorption) of the fresh calcined samples.

Sample	$S.A._{BET}$ ($m^2\,g^{-1}$)[a]	V_s ($cm^3\,g^{-1}$)[b]	H_2 uptake ($mol\,g^{-1} \times 10^{-3}$)[c]	H_2/Cu ($mol\,mol^{-1}$)[c]	O_{2des} ($\mu mol\,O_2\,g^{-1}$)[d]	T_1 (°C)	O_{2des} ($\mu mol\,O_2\,g^{-1}$)[d]	T_2 (°C)
FCZCu	28 ± 1	0.02	1.08	1.21	56	123	250	786
CZCu	19 ± 1	0.05	1.04	1.18	53	104	329	786
FCCu	22 ± 1	0.02	1.22	1.02	39	112	356	805
CCu	25 ± 1	0.21	1.39	1.16	51	113	340	800

[a] BET specific surface area.
[b] Specific pore volume at $P/P_0 = 0.98$.
[c] By H_2-TPR analysis.
[d] By O_2-TPD analysis.

O_2-TPD analysis was carried out study the release of oxygen from the Cu containing materials. A preliminary study was carried out on pure ceria. The pure ceria O_2-TPD profile shows a broad peak centered at 104 °C attributable to surface adsorbed oxygen species.

All the O_2-TPD profiles of the studied catalysts show two peaks, the first at about 110 °C and the second at about 800 °C (Fig. 5).

The low temperature broad TPD peak can be attributed to desorption of surface adsorbed oxygen species and the second can be due to desorption of lattice oxygen as consequence of the Cu reduction process, according to the reactions:

$$CuO \rightarrow Cu + 1/2O_2 \quad (1)$$

$$CuO \rightarrow 1/2Cu_2O + 1/4O_2 \quad (2)$$

The TPD profiles of all samples appear quite similar. Also the oxygen releases, obtained from the calculated area of the low temperature TPD peak, are similar for all the samples with the only exception of that of the sample FCCu, that shows a 30% reduced oxygen release in comparison with the other ones. The samples differ also for the amount of oxygen released at high temperature. Theoretically a sample containing 7.0 wt.% of Cu^{2+} must release 220.0 and 440 μmol O_2/g to give respectively the partial reduction to Cu^+ or the total reduction to metallic Cu (Table 1).

The sample FCZCu releases at high temperature an oxygen amount considerably lower than what required for the complete reduction of Cu^{2+} to metallic Cu. This could mean that in the zirconium doped sample FCZCu with flower-like morphology the copper sites are stabilized as partially charged species $Cu^{(2-\delta)+}$ with a formal oxidation state $Cu^+ < Cu^{(2-\delta)+} < Cu^{2+}$. Moreover some reduction to metallic copper is observed also in the O_2-TPD profile of the other samples CZCu, FCCu, CCu but not in that of FCZCu.

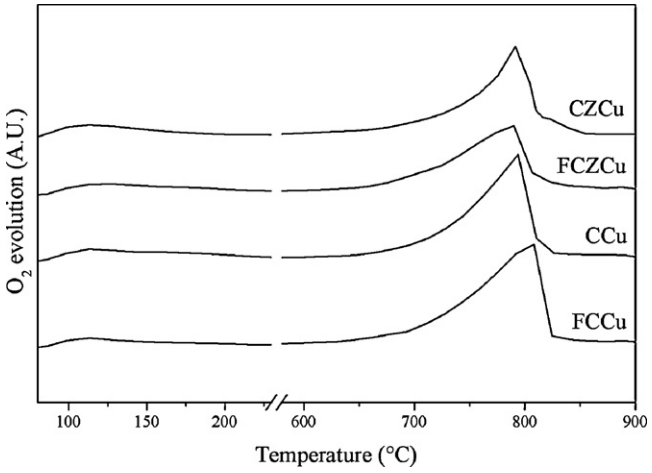

Fig. 5. O_2-TPD profiles of the indicated samples.

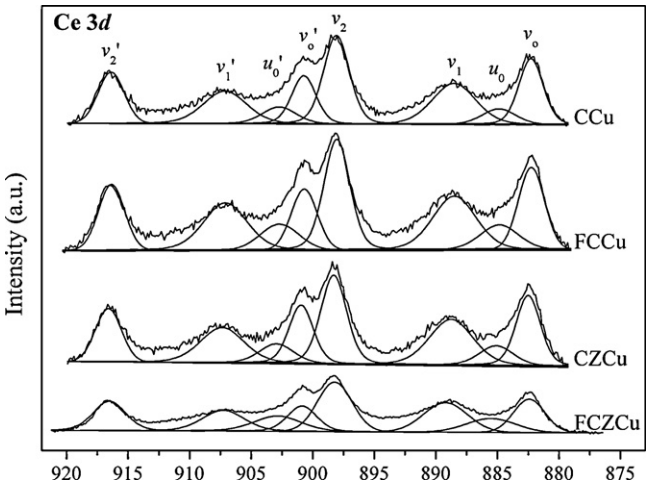

Fig. 6. Ce 3d photoelectron profiles of indicated samples.

3.4. XPS

XPS was used to study the chemical state of the elements and their relative abundance in the catalyst surface. The Ce 3d and Cu 2p signals are of particular interest to know the chemical state of the active phase. Fig. 6 shows the XPS Ce 3d spectra of the studied samples. The interpretation of the core level Ce 3d spectra is difficult due to the hybridization between the Ce 4f levels and the O 2p states [38]. A detailed description of the Ce 3d spectra for Ce^{4+} and Ce^{3+} from CeO_2 and Ce_2O_3, respectively, has been reported [52] and it is possible to estimate the reduction degree of ceria by considering the relative intensity of the u_0 (v_0) and u' (v') peaks to the intensity of Ce 3d region [53]:

The percentages of reduced cerium ions (Ce^{3+}) for the studied samples are compiled in Table 2 and are more or less the same for samples CCu, FCCu and CZCu, whereas the Ce reduction degree appears to be much higher (21%) for the sample FCZCu.

The presence of surface carbonates was detected at 288.3–288.7 eV in the C 1s core level signal of all samples, close to the reference signal of adventitious carbon at 284.8 eV. The presence of surface carbonates is always observed on the surface of lanthanide oxides. The O 1s core level spectra show an asymmetric peak that can be decomposed in two contributions at 529.0–529.6 eV and 531.3–531.7 eV assigned to ceria and copper

Table 2
Redox parameters determined by XPS.

Sample	Cu $2p_{3/2}$	I_{sat}/I_{mp}	Zr/Ce	Cu/Ce	$\%Ce^{3+}$
CCu	932.3 (46%)934.0 (54%)	0.46	–	0.38	10.6
FCCu	931.9 (36%)933.8 (64%)	0.49	–	0.39	13.0
CZCu	933.6	0.53	0.42	0.49	11.4
FCZCu	932.6 (78%)934.8 (22%)	0.28	0.07	0.33	21.0

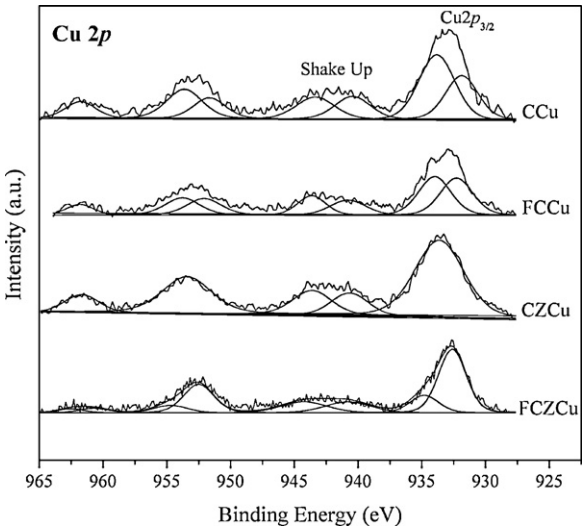

Fig. 7. Cu 2p photoelectron profiles of studied samples.

oxides, respectively. Zr $3d_{5/2}$ core levels spectra have maxima at 182.1 eV, assigned to Zr^{4+}.

The presence of reduced copper species can be estimated by the ratio between the intensity of the shake-up satellite peak and the main Cu $2p_{3/2}$ peak (see Fig. 7 and Table 2). All catalysts show a I_{sat}/I_{mp} value lower than that observed for CuO (0.55), indicating the presence of partially reduced copper species [23,54], except in the case of sample CZCu, where no reduction of Cu^{2+} is observed and the found I_{sat}/I_{mp} value (0.53) is very close to that of for CuO. The sample FCZCu, with the lowest I_{sat}/I_{mp} value (0.28), in agreement with O_2-TPD data of the amount of high temperature released oxygen, resulted to have the highest degree of copper reduction.

3.5. CO preferential oxidation activity

The catalytic activity of the samples was evaluated in the CO-PROX reaction and the results of the experiments in the 40–190 °C temperature range, carried out using a synthetic reformate gas (1.25% CO, 1.25% O_2, 50.0% H_2, He balance), are presented in Fig. 8a and b. All samples were tested twice. The second catalytic cycle was carried out using the same conditions used in the first one, that is: the used sample was heated again in situ at 400 °C under flowing filtered atmospheric air for 1 h and tested using the already mentioned conditions.

The second reaction profile was in all cases identical to the first one (graphic is not shown).

Lets analyze first the catalysts behavior in the lower temperatures range 40–140 °C and successively that above 140 °C. The value of T_{50} (temperature at which 50% of CO conversion is reached) is very similar for FCZCu, CZCu and CCu being 78 °C for the first and 80 °C for the other two samples (Fig. 8a). On the contrary the FCCu sample reaches the 50% of CO conversion only above 105 °C. The FCZCu catalysts reach 90% conversion at 103 °C, CZCu and CCu at 108 °C, while FCCu achieves this value only at 134 °C. The conversion maximum (>99.0%) of FCZCu, CZCu and CCu samples is reached at 140 °C while the CO conversion at this temperature is about 95% if FCCu is used. Above 140 °C, the activity of CZCu and CCu decreases with an almost identical trend, and more slowly in the case of FCZCu. The behavior of FCCu is quite different, because its activity increases up to >99.0% at 160 °C, then remaining constant till the end of the experiment.

It can also be noticed that, for all four samples, the selectivity to CO_2 is 100% below 90 °C (Fig. 8b).

Above this temperature, the selectivity falls down, more or less steeply, to values near 50% due to the strong competition between H_2 and CO for the reaction with O_2. In fact, as reported in literature [19,55], although both H_2 and CO oxidation should occur on the same active centers (basically the CuO/CeO_2 pairs in interfacial positions), they practically do not compete until relatively high temperatures, at which the chemisorption of the incoming molecules is weaker, are reached. Consequently, when $CuO–CeO_2$ catalysts are used, a higher selectivity toward CO oxidation is usually found at lower temperatures, because in these conditions, copper oxides are more easily reduced by CO than by H_2 [19,49]. The decrease of the selectivity toward CO oxidation, usually observed at higher temperatures, is the result of the simultaneous oxidation of CO and H_2, attributable to the easier H_2 activation on the reduced by CO metal sites.

It is nowadays widely accepted that CO and H_2 oxidation by molecular oxygen catalyzed by metal oxides, in particular nanostructured $Cu_xCe_{1-x}O_2$, proceeds by a redox mechanism, the kinetic of which was studied in detail by Sedmak et al. [56].

It was also demonstrated that Cu^{1+} species are stabilized by the interaction of the copper clusters with cerium oxide, this last playing the role of oxygen source [4,49,55,57], inducing various authors to claim that the close redox interaction between cerium and copper is the key factor responsible for the remarkable catalytic performances in the CO oxidation of Cu/Ce based catalysts [7,44,58–60] The strongly reactive interface zones between the metal and the support [61–63] represent most probably the active sites where the concomitant oxidation state changes of the metal ($Cu^{2+} \leftrightarrow Cu^{1+}$) and the support ($Ce^{3+} \leftrightarrow Ce^{4+}$) occur [56].

The synergistic effects of copper and ceria in the nanostructured Cu/Ce based catalytic systems can be summarized by the equilibrium $Ce^{4+} + Cu^{1+} \leftrightarrow Ce^{3+} + Cu^{2+}$ that is supposed to stabilize the cationic copper species in a strongly reductive environment by a buffer-like effect [56].

In the lower temperatures range 40–140 °C, the samples FCZCu, CCu, CZCu were found to behave quite differently from FCCu, as exemplified by their T_{50} (temperature at which half of the fed CO is consumed) values. The higher T_{50} value of FCCu can be correlated to absence in its H_2-TPR profile of the low temperature peaks, attributable to the reduction of easily reducible highly dispersed copper species doped in the ceria lattice, that are present in the profiles of the other three samples [51]. Also the XRPD data (Fig. 3) confirm that highly dispersed copper species are not present in the FCCu sample, which contains the 96% of all the copper as CuO crystallites with an average size of 14.0 nm. It can also be pointed out that the low temperature oxygen release of FCCu, as determined by O_2-TPD, is 30% less than what observed for the other three samples FCZCu, CCu, CZCu. The O_2-TPD profile of FCCu not only highlights the inferior oxygen adsorption capacity of this sample (Table 1, Fig. 5) but shows also that FCCu has the highest value of high temperature desorbed oxygen, ascribable to the presence of a bigger amount of copper in a high oxidation state. It can be also observed that the H_2-TPR profile of FCCu does not show any hydrogen consumption peak below 100 °C, usually attributable [47] to surface hydrogen chemisorption. Since it is generally accepted that surface-adsorbed oxygen and hydrogen together with lattice oxygen are involved in oxidation reactions in hydrogen rich gas streams, these data can justify the inferior catalytic activity shown by FCCu catalyst in the lower temperature region.

The FCZCu sample, with flower like micro-morphology, shows the most interesting catalytic behavior, with a T_{50} of 78 °C, a quite wide window (120–180 °C) of high (90–100%) CO conversion, with a CO_2 selectivity of almost 99% up to 120 °C. It must be pointed out that the O_2-TPD measurements show that this sample releases an amount of chemisorbed oxygen inferior to what would have been necessary to reduce all Cu^{2+} to Cu^0, most probably because some, if

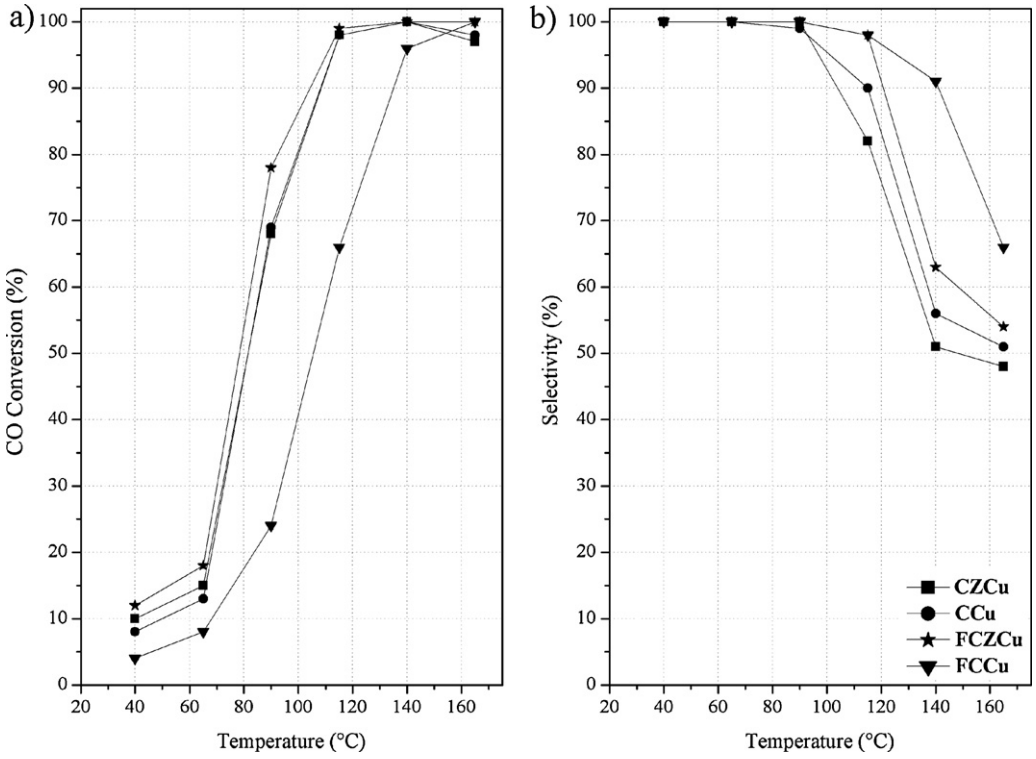

Fig. 8. Dependencies of: (a) CO conversion (%) and (b) selectivity to CO_2 (%) as a function of temperature. Operating conditions: GHSV = 22,000 h^{-1}; λ = 2; 1.25% CO, 1.25% O_2, 50% H_2, He balance (vol.%).

not all, copper is stabilized in an intermediate ($Cu^{(2-\delta)+}$) oxidation state (Section 3.3). The XPS measurements (Table 2), while showing that all catalysts have a I_{sat}/I_{mp} value lower than that observed for CuO (0.55), indicating the presence of partially reduced copper species, also point out that the FCZCu sample has the highest percentage of reduced copper species (Cu^{+}), together with the highest percentage (21%) of reduced (Ce^{3+}) cerium species. Also the Zr/Ce ratio of this sample measured by XPS is 0.07, i.e. much lower of that of the compositionally equivalent but morphologically disordered CZCu sample (0.42).

All samples were analyzed by XRPD after a CO-PROX cycle and, in all diffractograms (not shown), the size of ceria crystallites did not change during the reaction. On the contrary a small broad diffraction peak at 43.5° of 2θ, attributable to a metallic Cu phase, was detected in the XRPD patterns of the catalysts CZCu (2.2 wt.%), CCu (4.2 wt.%) and FCCu (5.2 wt.%), evidencing the occurred reduction of some of the copper during the reaction (Table 3). On the other hand no modification in the XRPD profile of the zirconium containing sample with flower-like morphology FCZCu was observed after reaction: in fact the same CuO amount (2.2 wt.%) was found both in the fresh and used catalyst.

Table 3
Weight% of CuO and Cu^0 as measured by XRPD for the studied catalysts before (fresh) and after (used)[a] reaction. Cu% is the percentage of the introduced total copper present as CuO or Cu^0.

Sample	CuO (wt.%)				Cu^0 (wt.%)			
	Fresh		Used		Fresh		Used	
	wt.%	Cu%	wt.%	Cu%	wt.%	Cu%	wt.%	Cu%
CCu	4.9	70	–	–	–	–	4.2	75
FCCu	6.8	97	–	–	–	–	5.2	93
CZCu	2.4	34	–	–	–	–	2.2	40
FCZCu	2.2	31	2.2	31	–	–	–	–

[a] The sample, after the catalytic test was cooled to RT in flow of gas with the same composition of the feed used in the reactivity measurements. The XRD analysis of all samples was carried out in air.

The analysis of the data obtained from all this set of measures enables some comments. First of all, the important role played by ceria doping with zirconium ions is confirmed [8,10–16,38]. It is in fact generally accepted that the oxidation of CO to CO_2 on ceria involves the participation of lattice oxygen species and it seems that the introduction of small amounts of zirconia in the ceria lattice causes an increase of structural defects with a consequent rise of the amount of oxygen that can be reversibly exchanged between the solid and the incoming reactive gas stream. The flower-like FCZCu material is slightly more performing than the morphologically disordered ceria–zirconia CZCu and ceria-only CCU. On the other hand CCu, FCCu and FCZCu show a very similar behavior below 140 °C, but it can also be observed that the two morphologically ordered FCZCu and FCCu samples maintain high CO conversion levels above 160 °C, with the FCZCu activity remaining constant at about 100% up to 190 °C, while the two CZCu and CCu samples show a sharp activity decay above 160 °C. Nevertheless the selectivity to CO_2 of all samples sharply decreases above 90 °C, with the exception of FCZCu that remains still selective (98%) up to 115 °C.

In order to check the effect of the reformate species CO_2 and H_2O on catalyst activity, 15% CO_2 and 10% H_2O (vol.%) were simultaneously added to the feed stream (Fig. 9). The negative effect of the presence of these two species in the feed, on the catalyst activity is evident if the conversion and selectivity data plotted in Figs. 9 and 8 are compared. An increase of almost forty degrees in the T_{50} values is in fact observed for all the samples.

The activity modification, exemplified by the T_{50} value, after water and carbon dioxide addition to the feed, is similar for all samples, following the ΔT_{50} trend (40) CZCu > (38) CCu ∼ (37) FCZCu > (34) FCZCu.

This is in agreement with what reported for similar CuO/CeO_2 catalysts, where this effect is ascribed to competitive adsorption of CO_2/CO and to the blocking effect of water [64–66]. The

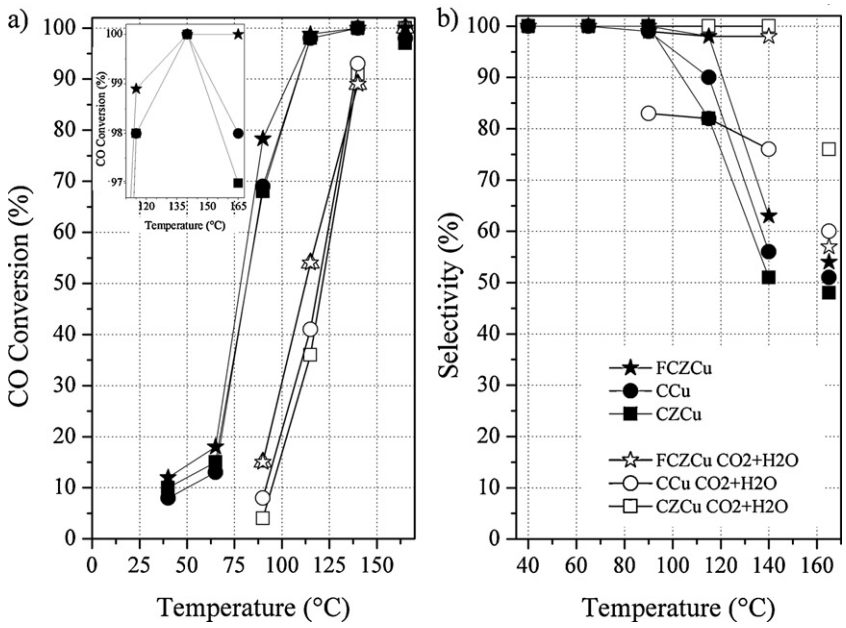

Fig. 9. Dependencies of the (a) CO conversion and (b) selectivity toward CO_2 as a function of temperature over the title catalysts, before and after the addition to the standard feed of 15 vol.% of CO_2 and 10 vol.% H_2O. Operating conditions: GHSV = 22,000 h^{-1}; $\lambda = 2$; 1.25% CO, 1.25% O_2, 50% H_2, 0–15% CO_2, 0–10% H_2O, He balance (vol.%). The inset of (a) shows an enlargement of the 110–150 °C temperature range for conversion values from 97% to 100%.

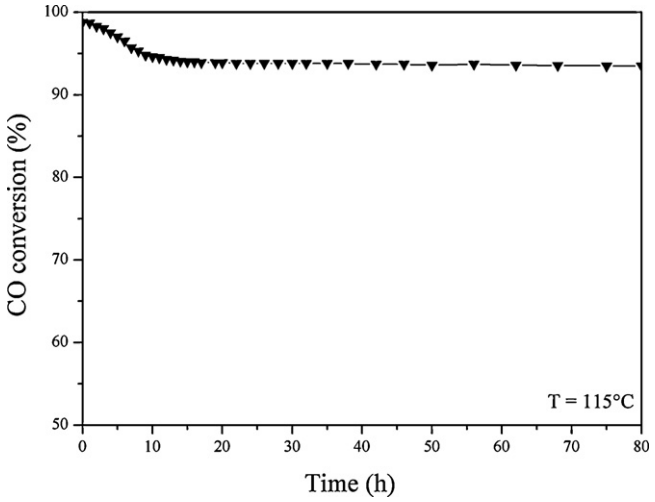

Fig. 10. Durability test at 115 °C carried out for the sample FCZCu (only the 0–80 h range is shown, because the conversion remains the same up to 150 h).

blocking effect of water and the decreased CuO–CeO_2 interfacial redox activity, caused by carbonates formation from adsorbed CO_2 on interfacial ceria sites, was also proved by Martinez-Arias by operando-DRIFT spectroscopy [67].

A durability test was performed on FCZCu and the conversion graphic is shown in Fig. 10. The reaction was monitored for 150 h maintaining the temperature constant at 115 °C, using GHSV = 22,000 h^{-1}; $\lambda = 2$; 1.25% CO, 1.25% O_2, 50% H_2, He balance (vol.%). The catalyst showed a diminution of CO conversion from 98% to 94% within the first 6 h, remaining stable for the further operation time.

Concluding, CeO_2–CuO catalytic systems are confirmed as very active and selective toward the oxidation of CO in hydrogen rich gas streams at quite low temperatures (80–120 °C). The observed high catalytic activity appears to be related to the presence of a large amount of highly reducible copper species closely interacting with the ceria surface. The role of Zr doping, in particular of Zr/Ce ratio, is less clear and surely needs further investigation, because a similar activity is observed in the samples FCZCu, CZCu and CCu. The FCZCu sample, prepared by slow precipitation, appears to have quite unique properties of activity, selectivity and stability that can be correlated to its micro-morphology and surface composition. As shown by SEM and TEM data, this sample has a regular layered flower like crystal morphology. The surface of this sample is Ce enriched (Zr/Ce= 0.07 compared to 0.42) and probably exposes for the most part the (1 1 0) plane. For Cu/Ce/Zr systems, these planes are known [21] to adsorb more easily the small molecules, and to stabilize cationic copper species. No copper reduction to metal was in fact observed in this sample after reaction. Very surprising was to find the activity of the not containing Zr sample FCCu, much lower of the other three and can be tentatively attributed to the prevailing formation of catalytically less active large CuO particles, probably favored by the absence of Zr and the slowness of the synthetic procedure. Further studies are planned in the near future to better investigate the role of the chemical composition for samples prepared by this simple and low-cost synthetic strategy.

Acknowledgements

The authors wish to thank Martina Marchiori (Ca' Foscari University – Venice) for N_2 physisorption and TPR-TPO measurements and Dr. Davide Cristofori (Ca'Foscari University-Venice) for the HRTEM measurements.

References

[1] H.H. Kung, M.C. Kung, Topics in Catalysis 34 (2005) 77.
[2] W.T. Wallace, B.K. Min, D.W. Goodman, Topics in Catalysis 34 (2005) 17.
[3] S. Royer, D. Duprez, ChemCatChem 3 (2011) 24.
[4] W. Liu, M. Flytzani-Stephanopoulos, Journal of Catalysis 153 (1995) 304.
[5] L. Kundakovic, M. Flytzani-Stephanopoulos, Applied Catalysis A 171 (1998) 13.
[6] G. Avgouropoulos, T. Ioannides, H. Matralis, Applied Catalysis B 56 (2005) 87.
[7] A. Martínez-Arias, A.B. Hungría, G. Munuera, D. Gamarra, Applied Catalysis B 65 (2006) 207.
[8] T. Caputo, R. Pirone, G. Russo, Kinetics and Catalysis 47 (2006) 761.
[9] E. Moretti, M. Lenarda, L. Storaro, A. Talon, R. Frattini, S. Polizzi, E. Rodríguez-Castellón, A. Jiménez-López, Applied Catalysis B 72 (2007) 149 (references therein).

[10] P. Fornasiero, G. Balducci, R. Di Monte, J. Kašpar, V. Sergo, G. Gubitosa, A. Ferrero, M. Graziani, Journal of Catalysis 164 (1996) 173.
[11] A. Martinez-Arias, M. Fernández-Garcia, O. Gálvez, J.-M. Coronado, J.A. Anderson, J.C. Conesa, J. Soria, G. Munera, Journal of Catalysis 195 (2000) 207.
[12] J.-L. Cao, Q.-F. Deng, Journal of Materials Science 44 (2009) 6663.
[13] M.P. Yeste, J.C. Hernández, S. Trasobares, S. Bernal, G. Blanco, J.J. Calvino, J.A. Pérez-Omil, J.M. Pintado, Chemistry of Materials 20 (2008) 5107.
[14] Y. Nagai, T. Yamamoto, T. Tanaka, S. Yoshida, T. Nonaka, T. Okamoto, A. Suda, M. Sugiura, Topics in Catalysis 47 (2008) 137.
[15] I. Atribak, N. Guillén-Hurtado, A. Bueno-López, A. García- García, Applied Surface Science 256 (2010) 7706.
[16] S. Abdollahzdeh-Ghom, C. Zamani, T. Andreu, M. Epifani, J.R. Morante, Applied Catalysis B 108–109 (2011) 32.
[17] P. Ratnasamy, D. Srinivas, C.V.V. Satyanarayana, P. Manikandan, R.S. Senthil Kumaran, M. Sachin, V.N. Shetti, Journal of Catalysis 221 (2004) 455.
[18] M. Manzoli, R. Di Monte, F. Boccuzzi, S. Coluccia, J. Kašpar, Applied Catalysis B 61 (2005) 192.
[19] X.-F. Dong, H.-B. Zou, W.-M. Lin, International Journal of Hydrogen Energy 31 (2006) 2337.
[20] E. Moretti, L. Storaro, A. Talon, R. Moreno-Tost, E. Rodríguez-Castellón, A. Jiménez-López, M. Lenarda, Catalysis Letters 129 (2009) 323.
[21] J. Zhu, L. Zhang, Y. Deng, B. Liu, L. Dong, F. Gao, K. Sun, L. Dong, Y. Chen, Applied Catalysis B 96 (2010) 449.
[22] Á. Reyes-Carmona, A. Arango-Díaz, E. Moretti, A. Talon, L. Storaro, M. Lenarda, A. Jiménez-López, E. Rodríguez-Castellón, Journal of Power Sources 196 (2011) 4382.
[23] H.X. Mai, L.D. Sun, Y.W. Zhang, R. Si, W. Feng, H.P. Zhang, H.C. Liu, C.H. Yan, Journal of Physical Chemistry B 109 (2005) 24380.
[24] K.B. Zhou, X. Wang, X.M. Sun, Q. Peng, Y.D. Li, Journal of Catalysis 229 (2005) 206.
[25] R. Si, M. Flytzani-Stephanopoulos, Angewandte Chemie International Edition 47 (2008) 2884.
[26] W.I. Hsiao, Y.S. Lin, Y.C. Chen, C.S. Lee, Chemical Physics Letters 441 (2007) 294.
[27] G. Yia, Z. Xu, G. Guo, K. Tanaka, Y. Yuan, Chemical Physics Letters 479 (2009) 128.
[28] G.-R. Li, D.-L. Qu, Y.-X. Tong, Journal of Physical Chemistry C 113 (2009) 2704.
[29] L.-L. Ma, J.-L. Li, H.-Z. Sun, M.-Q. Qiu, J.-B. Wang, J.-Y. Chen, Y. Yu, Materials Research Bulletin 45 (2010) 961.
[30] Z. Cheng, J. Xu, H. Zhong, X. Chu, J. Song, Materials Letters 65 (2011) 2047.
[31] S. Ashoka, G. Nagaraju, C.N. Tharamani, G.T. Chandrappa, Materials Letters 63 (2009) 873.
[32] Y. Lai, M. Meng, Y. Yu, X. Wang, T. Ding, Applied Catalysis B 105 (2011) 335.
[33] Y. Lu, L. Wang, D. Wang, T. Xie, L. Chen, Y. Lin, Materials Chemistry and Physics 129 (2011) 281.
[34] L.-S. Zhong, J.-S. Hu, H.-P. Liang, A.-M. Cao, W.-G. Song, L.-J. Wan, Advanced Materials 18 (2006) 2426.
[35] L.-X. Yang, Y.-J. Zhu, L. Li, L. Zhang, H. Tong, W.-W. Wang, G.-F. Cheng, J.-F. Zhu, European Journal of Inorganic Chemistry (2006) 4787.
[36] L. Zhou, J. Zhang, J. He, Y. Hu, H. Tian, Materials Research Bulletin 46 (2011) 1714.
[37] H. Li, G. Lu, Y. Wang, Y. Guo, Y. Guo, Catalysis Communications 11 (2010) 946.
[38] E. Moretti, L. Storaro, A. Talon, M. Lenarda, P. Riello, R. Frattini, M. Martínez de Yuso, A. Jiménez-López, E. Rodríguez-Castellón, F. Ternero, A. Caballero, J.P. Holgado, Applied Catalysis B 102 (2011) 627.
[39] S. Poulston, P.M. Parlett, P. Stone, M. Bowker, Surface and Interface Analysis 24 (1996) 811.
[40] X. Wang, J.A. Rodriguez, J.C. Hanson, D. Gamarra, A. Martinez-Arias, M. Fernandez-Garcia, Journal of Physical Chemistry 109 (2005) 19595 (references therein).
[41] G. Aguila, F. Gracia, P. Araya, Applied Catalysis A: General 343 (2008) 16.
[42] Y.-Z. Chen, B.J. Liaw, H.-C. Chen, International Journal of Hydrogen Energy 31 (2006) 427.
[43] A. Martínez-Arias, D. Gamarra, M.Fernández-García, A. Hornés, P. Bera, Z. Koppány, Z. Schay, Catalysis Today 143 (2009) 211.
[44] T. Caputo, L. Lisi, R. Pirone, G. Russo, Applied Catalysis A 348 (2008) 42.
[45] A. Pintar, J. Batista, S. Hočevar, Journal of Colloid and Interface Science 285 (2005) 218.
[46] S. Piras, A. Colussi, A. Trovarelli, V. Sergo, J. Llorca, R. Psaro, L. Sordelli, Journal of Physical Chemistry B 109 (2005) 11110.
[47] P. Zimmer, A. Tschöpe, R. Birringer, Journal of Catalysis 205 (2002) 339.
[48] R. Pérez-Hernándes, A. Gutiérrez-Martínez, C.E. Gutiérrez-Wing, International Journal of Hydrogen Energy 32 (2007) 2888 (references therein).
[49] D. Gamarra, A. Hornés, Z. Koppány, Z. Schay, G. Munuera, J. Soria, A. Martinez-Arias, Journal of Power Sources 169 (2007) 110.
[50] E. Moretti, L. Storaro, A. Talon, P. Riello, R. Frattini, M. Lenarda, Microporous and Mesoporous Materials 116 (2008) 575.
[51] J. Beckers, G. Rothemberg, Dalton Transactions 37 (2008) 6573.
[52] F. Larachi, J. Pierre, A. Adnot, A. Bernis, Applied Surface Science 195 (2002) 236.
[53] X. Tang, B. Zhang, Y. Li, Y. Xu, Q. Xin, W. Shen, Applied Catalysis A 288 (2005) 116.
[54] G. Avgouropoulos, T. Ioannides, Applied Catalysis B 67 (2006) 1.
[55] S. Hocevar, U.O. Krasovec, B. Orel, A.S. Arico, H. Kim, Applied Catalysis B 28 (2000) 113.
[56] G. Sedmak, S. Hočevar, J. Levec, Journal of Catalysis 213 (2003) 135.
[57] H. Zhou, X. Dhong, W. Lin, Applied Surface Science 253 (2006) 2893.
[58] A. Martinez-Arias, M. Fernandez-Garcia, A.B. Hungria, A. Iglesias-Juez, O. Galvez, J.A. Anderson, J.C. Conesa, J. Soria, G. Munuera, Journal of Catalysis 214 (2003) 261.
[59] A. Martinez-Arias, A.B. Hungria, M. Fernandez-Garcia, J.C. Conesa, G. Munuera, Journal of Physical Chemistry B 65 (2006) 207.
[60] A. Gurbani, J.L. Ayastuy, M.P. González-Marcos, M.A. Gutiérrez-Ortiz, International Journal of Hydrogen Energy 35 (2010) 11582.
[61] A. Trovarelli, Catalysis Reviews: Science and Engineering 38 (1996) 439.
[62] M. Primet, E. Garbowski, in: A. Trovarelli (Ed.), Catalysis by Ceria and Related Materials, Catalysis Science Series, vol. 2, Imperial College Press, London, 2002.
[63] M. Boaro, M. Vicario, C. de Leitenburg, G. Dolcetti, A. Trovarelli, Catalysis Today 77 (2003) 407.
[64] T. Caputo, L. Lisi, R. Pirone, G. Russo, Industrial and Engineering Chemistry Research 46 (2007) 6793.
[65] E. Moretti, M. Lenarda, L. Storaro, A. Talon, T. Montanari, G. Busca, E. Rodrıguez-Castellon, A. Jimenez-Lopez, M. Turco, G. Bagnasco, R. Frattini, Applied Catalysis A 335 (2008) 46.
[66] G. Avgouropoulos, T. Ioannides, Applied Catalysis A 244 (2003) 155.
[67] D. Gamarra, A. Martinez-Arias, Journal of Catalysis 263 (2009) 189.